Human Molecular Genetics, 2009, Vol. 18, No. 11 ***1962–1975***
doi:10.1093/hmg/ddp117
Advance Access published on March 13, 2009

Identification of interactive networks of gene expression associated with osteosarcoma oncogenesis by integrated molecular profiling

Bekim Sadikovic[1,†], Maisa Yoshimoto[2,†], Susan Chilton-MacNeill[1], Paul Thorner[1], Jeremy A. Squire[2,*] and Maria Zielenska[1]

[1]Department of Pediatric Laboratory Medicine, The Hospital for Sick Children, Toronto, Canada M5G 1X8 and [2]Department of Pathology and Molecular Medicine, Richardson Laboratories, Kingston General Hospital, Queen's University, 88 Stuart Street, Kingston, Ontario, Canada K7L 3N6

Received January 30, 2009; Revised February 19, 2009; Accepted March 9, 2009

Altered gene expression in tumors can be caused by copy number alterations to DNA or mutation affecting coding or regulatory regions of genes. However, epigenetic events may also influence gene expression. Malignant cells can show major disruptions in DNA methylation profiles, which are manifested as aberrant hypermethylation or as hypomethylation of gene promoters, as well as global genomic hypomethylation. In this study we performed integrative whole-genome analysis of DNA copy number, promoter methylation and gene expression using 10 osteosarcomas. We identified significant changes including: hypomethylation, gain, and overexpression of histone cluster 2 genes at chromosome 1q21.1-q21.3; loss of chromosome 8p21.2-p21.3 and underexpression of *DOCK5* and *TNFRSF10A/D* genes; and amplification-related overexpression of *RUNX2* at chromosome 6p12.3-p21.1. Amplification and overexpression of *RUNX2* could disrupt G2/M cell cycle checkpoints, and downstream osteosarcoma-specific changes, such as failure of bone differentiation and genomic polyploidization. Failure of DOCK5-signaling, together with p53 and TNFRSF10A/D-related cell cycle and death pathways, may play a critical role in abrogating apoptosis. Our analyses show that the *RUNX2* interactome may be constitutively activated in osteosarcoma, and that the downstream intracellular pathways are strongly associated with the regulation of osteoblast differentiation and control of cell cycle and apoptosis in osteosarcoma.

INTRODUCTION

Hallmarks of cancer include deregulation of gene expression profiles and disruption of molecular networks as a result of the changes at the DNA level (1). However, it has become evident that epigenetic factors, particularly heritable changes in DNA methylation, can confer additional advantages to tumors that include deregulation of gene expression and destabilization of chromatin (2). While there is some understanding of how such genetic and epigenetic changes can influence gene expression, it is less clear how these mechanisms influence each other, and how cumulative changes could co-evolve and influence gene expression during tumorigenesis. As a result of advancements in microarray technologies, the relationships between changes in genomic content, epigenetics and gene expression can now be studied on a whole genome scale, allowing for substantial advancements in our understanding of genomic mechanisms influencing tumorigenesis (3–5).

Osteosarcoma is a pediatric bone tumor characterized by an unusually high frequency of genomic rearrangements. Molecular cytogenetic techniques together with the classical G-banded cytogenetic analysis of osteosarcoma tumors have described complex karyotypes with multiple numerical and structural chromosomal aberrations (6–12). Although genetic changes in this tumor have been extensively researched, our understanding of epigenetic changes in this tumor is limited. Aberrant DNA methylation of gene promoters has been shown in some osteosarcoma cell lines and tissues and include osteocalcin

*To whom correspondence should be addressed. Tel: +1 6135332345; Fax: +1 6135336830; Email: squirej@queensu.ca
†The authors wish it to be known that, in their opinion, the first two authors should be regarded as joint First Authors.

© *The Author 2009. Published by Oxford University Press. All rights reserved.*
For Permissions, please email: journals.permissions@oxfordjournals.org

Downloaded from https://academic.oup.com/hmg/article/18/11/1962/2527323 by guest on 20 August 2022

(13–15), *RASSF1* (16), imprinted *IGF2* and *H19* loci (17), and *GADD45A* gene (18,19).

In order to study the combined effects of genomic and epigenomic mechanisms on cancer-related gene networks, we recently developed an integrative approach for genome-wide high-resolution profiling of genetic, epigenetic and gene expression changes (20). These analyses provided evidence of the cumulative roles of epigenetic and genetic mechanisms in deregulation of gene expression networks in osteosarcoma cell lines. The objective of our current study was to apply this approach to a panel of primary osteosarcoma tumors, and to characterize the correlation between global changes in copy number, DNA methylation and gene expression, their influence on deregulation of core osteosarcoma gene networks, and to identify specific genes that are associated with the osteosarcoma phenotype, relative to normal human osteoblasts.

RESULTS

DNA copy number change, promoter methylation, and gene expression profiling of osteosarcoma tumors

In order to characterize genomic changes in osteosarcoma and identify tumor-specific genetic, epigenetic and expression profiles of all human genes, we used an integrative approach involving copy number array CGH profiling with Agilent 244K arrays, Me-DIP-chip methylation profiling of 10–12.5 kb promoter regions with Affymetrix Promoter Tilling Arrays, and gene expression analysis with Affymetrix Gene 1.0 Arrays. This integrative approach has allowed us to identify genomic regions, and specific genes with correlation between genetic and epigenetic alterations and their association with concurrent changes in gene expression. Copy number analysis was conducted in 10 primary tumor samples, six of which were used for gene expression and five for high-resolution DNA methylation profiling. Analyses were performed relative to normal human osteoblasts for methylation and expression, and relative to pooled normal DNA for copy number analysis. All array experiments were performed in duplicates. The high reproducibility of these analyses is evident in the immediately proximal clustering of the replicate experiments in the Principal Component Analysis (Supplementary Material, Fig. S1). Furthermore, copy number analysis revealed heterogeneity of the individual tumor samples (Supplementary Material, Fig. S1A), while expression (Supplementary Material, Fig. S1B) and DNA methylation (Supplementary Material, Fig. S1D) show distinct clustering of tumors relative to normal human osteoblasts. As expected, methylation arrays reveal separate clustering of arrays from input (IN) and immunoprecipitated (IP) fractions (Supplementary Material, Fig. S1C), which upon background normalization procedures show separate clustering between normal and tumor DNA methylation profiles (Supplementary Material, Fig. S1D).

Microarray and statistical analysis using Partek Genomic Suite (PGS) software resulted in the identification of epi/genomic and transcriptional alterations in individual tumor samples, and cumulative changes across all tumors (Supplementary Material, Tables S1–3). Integration of these data using Venn analysis revealed evidence of gene-specific overlap (Fig. 1A). Tumor-specific changes ranged between 2352 (T182) and 4170 (T177) genes for gene expression, between 907 (T179) and 2464 (T182) for DNA methylation, and 120 (T179) and 1910 (T178) for copy number. There were more hypermethylation events relative to hypomethylation in all tumors except T180, prevalence of copy number gain relative to loss in all but T178, and underexpression was over-represented relative to overexpression in all but T179 (Supplementary Material, Table S4). While these global integrative analyses revealed gene-specific overlaps between genomic mechanisms, subsequent inspection of chromosome-specific changes revealed evidence of correlation of such changes. For example, a region of recurrent genomic gain in chromosome 6p overlaps with the distinct cluster of gene over-expresson, while chromosome 5, which exhibits relatively normal genomic content, displays a distinct cluster of hypermethylated genes at q-arm that closely overlaps a cluster of gene underexpression (Supplementary Material, Fig. S2).

Combined effect of DNA copy number and differential methylation on gene expression

In order to characterize the correlations between gene-specific changes in the two-way intersects of the Venn analyses, we plotted these genes based on copy number, DNA methylation and gene expression status (Fig. 1B; Supplementary Material, Table S4). This analysis showed that strongest correlation was evident between copy number gain and overexpression, copy number loss and underexpression, and hypomethylation and copy number gains in most tumors (Fig. 1B). Furthermore, analysis of the three-way intersects revealed the strongest association between overexpression and hypomethylation of genes in regions of genomic gain (Fig. 1C). Pooled analysis of these genes showed that 49% exhibited overexpression, hypomethylation and copy number gain (Fig. 1D). Interestingly, 18% exhibited gene overexpression with concurrent hypermethylation and copy number gain, suggesting the dominance of copy number change relative to epigenetic change, in the ability to influence gene expression (Fig. 1D).

In order to identify the most significant recurrent genomic changes in OS, we performed cumulative analysis by comparing genomic profiles in all tumor samples relative to normal osteoblasts. We identified 1936 genes with significant changes in gene expression, 887 genes with changes in promoter DNA methylation, and 409 genes in regions of copy number imbalance (Fig. 2A; Supplementary Material, Tables S1–4). Genes with dual profile changes displayed a strong correlation between copy number gain and overexpression, copy number loss and underexpression, and hypomethylation and genomic gain (Fig. 2B; Supplementary Material, Table S5).

Gene network analysis

To identify osteosarcoma-related gene networks, we performed Ingenuity Pathway Analysis (IPA) of the genes identified in the cumulative DNA methylation, copy number and gene expression analyses. We compared the most significantly affected biological functions from gene expression analysis to the data obtained in the DNA methylation and copy number analyses (Fig. 2C). All tumors exhibited disruptions in gene expression in similar biological functions, with the most

Downloaded from https://academic.oup.com/hmg/article/18/11/1962/2527323 by guest on 20 August 2022

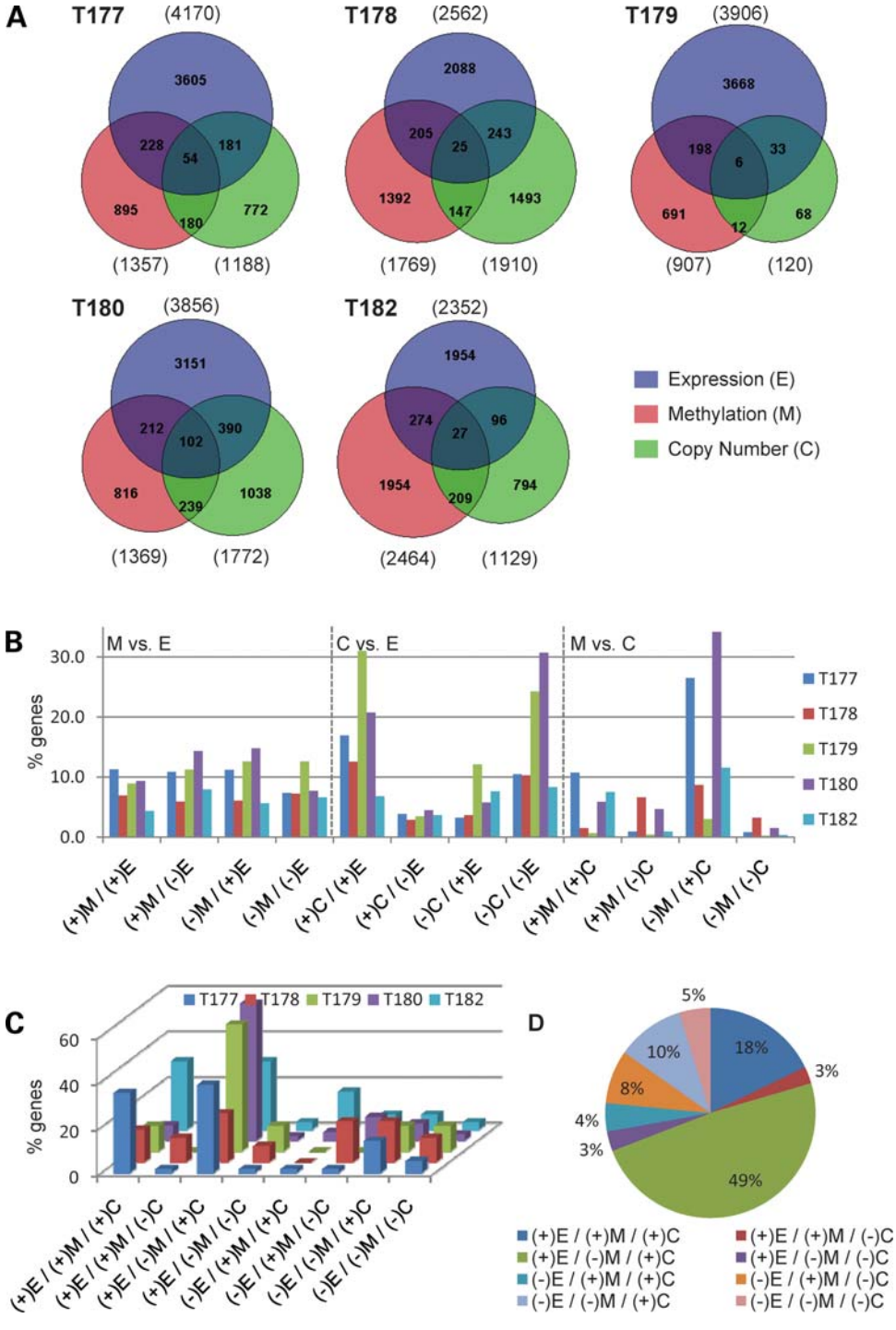

Figure 1. Integrative epi/genomic analysis of osteosarcomas. (**A**) Integration of expression, DNA methylation and copy number data in osteosarcoma tumors. Genes with significant changes in copy number, and DNA methylation and gene expression relative to normal human osteoblasts in individual tumor samples were analyzed using PGS-Venn analysis tool. The numbers in brackets indicate total number of genes showing significant changes, as described in Materials and Methods section. (**B**) Relative quantification of genes identified in two-way analysis. Line graph represents percentage of genes in the first variable relative to the total number of genes with specific changes in that variable (Fig. 1A; Supplementary Material, Table S1). For example, two-way analysis (+)C/(+)E for tumor sample 180 shows 20% genes, which indicates that 20% of the total 1339 genes with significant copy number gain (Supplementary Material, Table S1) also display significant gene overexpression. (**C**) Distribution of significant tumor-specific changes with changes in three of three (DNA methylation, copy number, gene expression) variables (three-way analysis). Percentage of genes (*y*-axis) identified with specific changes (*x*-axis) in the three-way intersect (A) for individual tumors is plotted. (**D**) Percentage distribution of three-way changes in DNA methylation, copy number and gene expression across all tumors. Total number of genes with specific three-way changes is added and represented as a percentage of the total number of genes with all variables of three-way changes.

Downloaded from https://academic.oup.com/hmg/article/18/11/1962/2527323 by guest on 20 August 2022

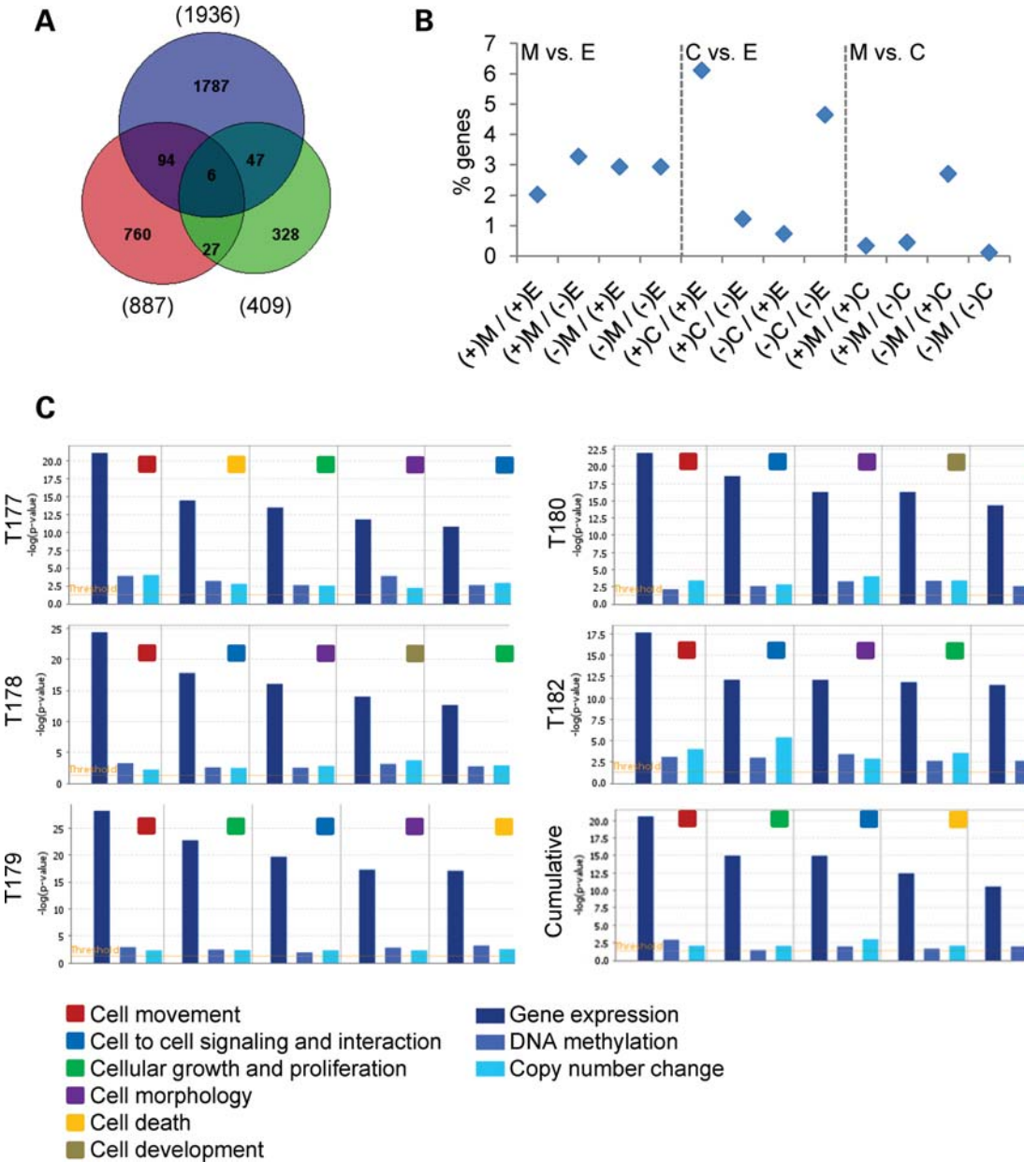

Figure 2. Analysis of gene-specific changes in DNA methylation, copy number and gene expression in osteosarcoma. (**A**) Integration of expression, DNA methylation and copy number data in osteosarcoma tumors identified by cumulative analysis using PGS-Venn analysis tool. The numbers in brackets indicate total number of genes showing significant changes in gene expression, copy number and DNA methylation, as described in Materials and Methods section. (**B**) Identification of genes with significant tumor-specific changes in two-way analysis of (DNA methylation, copy number, gene expression) variables. The columns represent the number of genes detected in the two-way intersects of the PGS-Venn analysis between DNA methylation, copy number and gene expression in individual tumors. M, methylation; C, copy number; E, expression; (−), loss of; (+), gain of. (**C**) Genes with methylation and copy number changes play a significant role in osteosarcoma-specific gene expression. Top five most significantly affected biological functions in individual osteosarcoma tumors and cumulative analysis relative to normal osteoblasts detected using the Ingenuity Pathway Analysis (IPA) Comparative Analysis tool. IPA analysis of gene expression (dark blue bars), DNA methylation (light blue bars) and copy number (turquoise bars). The *P*-value threshold is 0.05.

significant change in cell movement. Importantly, significant contribution ($P < 0.05$) of DNA methylation and copy number changes was detected across all biological functions in all tumors. We identified gene networks with most significant cumulative changes in gene expression (Supplementary Material, Table S6), DNA methylation (Supplementary Material, Table S7) and copy number (Supplementary Material, Table S8). The most significant gene expression networks included genes involved in organ and cellular development (network 1), p53-related cell death and cancer pathways (network 2), and DNA replication, recombination and repair (network 3; Fig. 3A). Correlations between copy number changes and gene expression, and copy number gain and DNA hypomethylation (Figs 1B and 2B), are clearly evident in the most significantly affected copy number-related gene network (Fig. 3B). Overlaying the gene expression data

Downloaded from https://academic.oup.com/hmg/article/18/11/1962/2527323 by guest on 20 August 2022

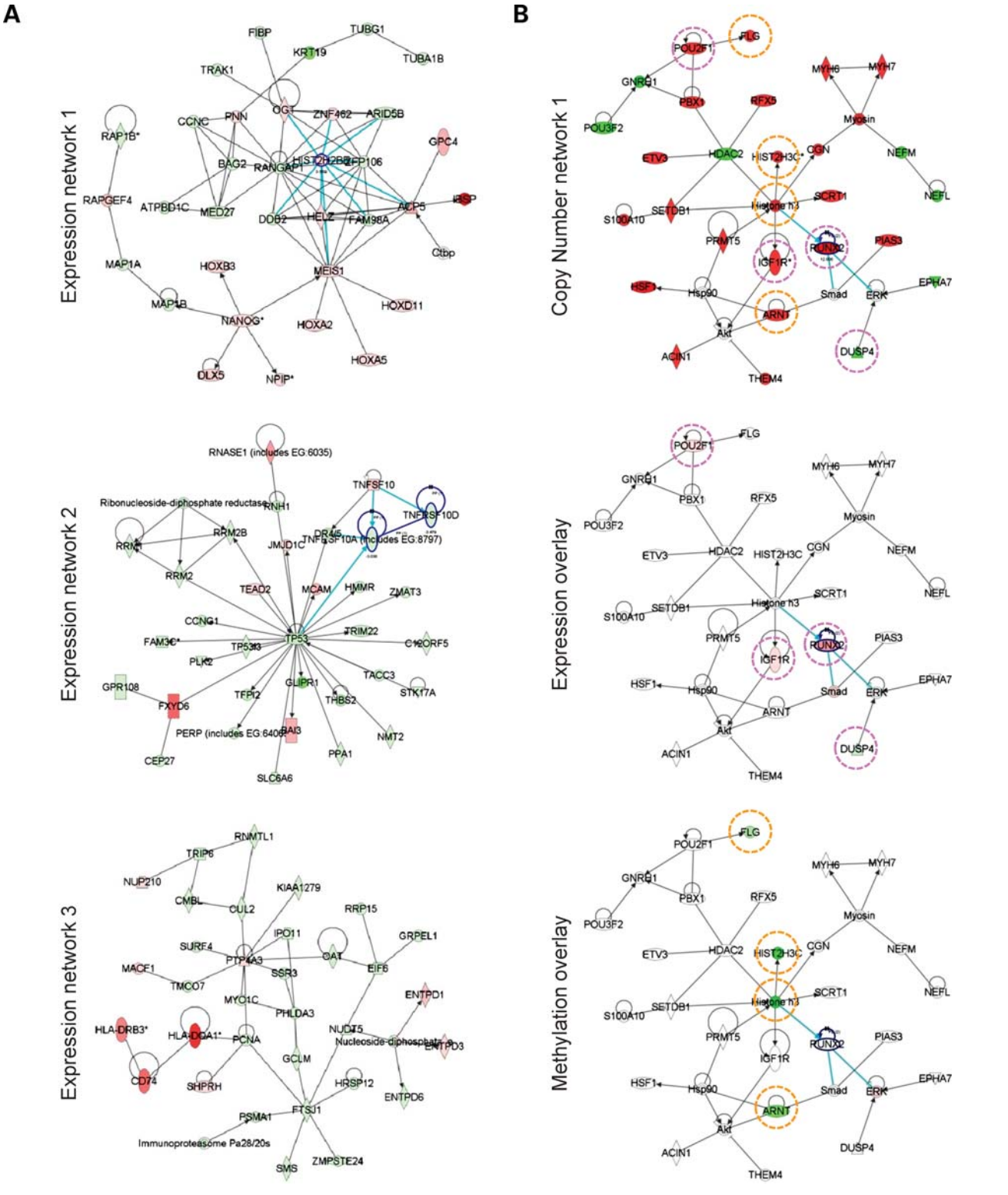

Figure 3. Epigenetic and genetic contribution to disruption of cellular functions and gene expression networks in osteosarcoma. (**A**) Ingenuity Pathway Analysis (IPA)-generated visualizations of top three most significantly affected gene expression networks in osteosarcoma (Supplementary Material, Table S5). Highlighted genes *HIST2H2BE* in network 1 and *TNFRSF10A* and *TNFRSF10D* are genes identified as significant using two-way and three-way correlation analysis. Red denotes gain, green denotes loss. (**B**) *RUNX2*-related changes in copy number, gene expression and DNA methylation in osteosarcoma tumors. IPA identified most significant copy number network is presented (top), with the IPA gene expression analysis overlay (middle), and IPA methylation analysis overlay (bottom). Red denotes gain, green denotes loss.

Downloaded from https://academic.oup.com/hmg/article/18/11/1962/2527323 by guest on 20 August 2022

Table 1. Candidate genes with OS-specific epi/genomic changes identified by integrative and gene network analyses

Genomic correlation	Genomic region	Genes of interest	Analysis results
Copy number gain and overexpression	6p12.3-p21.1	*RUNX2*	Most significant gain: 6/10 tumors 9-fold overexpression: 6/6 tumors Most significant copy number network 1 (IPA)
Copy number loss and underexpression	8p21.2-21.3	*DOCK5*	Most significant loss: 5/10 tumors 6-fold underexpression: 6/6 tumors
		TNFSRF10A/10D	Significant loss: 4/10 tumors 3/3.5-fold (10A/10D) underexpression: 6/6 tumors Second most significant expression network (IPA)
Hypomethylation and copy number gain	1q21.1-q21.2	*Histone cluster 2 genes*	Significant hypomethylation: cumulative analysis Significant copy number gain: 4/10 tumors Seven family members: HIST2-H2AA3/H2AAC/H2BE/H3C/H2AB/H4B/H2AA4 HIST2H2BE/H4B: gain, hypomethylation, overexpression (3.6-/4.8-fold: 6/6 tumors) HIST2H2BE: most significant expression network 1 (IPA)

to this network revealed that all genes with changes in copy number, including *RUNX2*, *SMAD*, *IGF1R* and *POU2F1* were also overexpressed in osteosarcoma tumors, while the only gene with copy number loss, *DUSP4*, shows underexpression (Fig. 3B; Supplementary Material, Table S5). Similarly, all hypomethylated genes in this network including *FLG*, *ARNT*, *HISTH3C* and *HIST2H3C* are in the region of copy number gain at chromosome 1q (Fig. 3B; Supplementary Material, Table S5). Furthermore, gene expression network 1 centers on *HIST2H2BE* gene (Fig. 3A), which was also detected in the three-way analysis as gained, hypomethylated and overexpressed (Supplementary Material, Table S5). Also, gene expression network 2 centers on the *TP53* gene and involves *TNFRSF10A* and *TNFRSF10D* genes that belong to the most significant region of loss at chromosome 8p and exhibit concurrent loss of gene expression (Fig. 3A; Supplementary Material, Table S5).

Identification of candidate genes using integrative genomic and functional network analysis

The next phase of the study was to identify differentially expressed groups of genes of direct relevance to established pathways of oncogenesis in osteosarcoma. This was achieved by combining the results from the PGS-based integrative genomic analyses (Supplementary Material, Table S5) and gene network analyses (Fig. 3; Supplementary Material, Table S6–8). We focused on genes with copy number-related deregulation of expression, and regions of genomic hypomethylation that were concurrent with gene amplification (Figs 1B and 2B). The candidate genes we identified are presented in Table 1. Amplification and overexpression was most evident at chromosomes 6p and 1q, where the most significantly amplified locus 6p12.3 (6/10 tumors) also showed 9-fold overexpression for gene *RUNX2* (Supplementary Material, Table S5). This gene is also part of the most significant copy number gene network (Fig. 3B). Deletion and underexpression was strongly associated with chromosome 8p and included *DOCK5* (5/10 tumors), *TNFRSF10A* (4/10 tumors) and *TNFRSF10D* (4/10 tumors), with 6-, 3- and 3.5-fold underexpression, respectively (Supplementary Material, Table S5). *TNFRSF10A* and *TNFRSF10D* genes are also part of the p53-related gene expression network involved in cancer and cell death (Fig. 3A). Amplification with concurrent DNA hypomethylation was prominent in the region adjacent to pericentromeric heterochromation of chromosome 1q, affecting 17 genes including seven members of the histone cluster 2 gene family at chromosome 1q21 (Supplementary Material, Table S5). *HIST2H2BE* and *HIST2H4B* were also identified in the three-way comparative analysis as significantly overexpressed (3.5- and 4.7-fold, respectively). Furthermore, *HIST2H2BE* is centrally located in the organ and cell development gene expression network (Fig. 3A).

Quantitative mass spectrometric analysis of hypomethylation of histone cluster 2 gene family

The histone cluster 2 gene family at chromosome 1q21 showed the strongest evidence of genomic gain-related DNA hypomethylation (Table 1). We validated hypomethylation in this region using quantitative mass spectrometric determination of bisulfite-treated DNA derived from two of the promoter-associated regions (21 and 22) that were identified as significantly hypomethylated using Me-DIP arrays (Fig. 4A). This analysis confirmed hypomethylation across most of the CpGs in all tumor samples, with as much as 60–70% loss of DNA methylation at some CpGs in T178 (Fig. 4B). Notably, T179, which showed the smallest changes in DNA methylation relative to normal human osteoblasts, also displayed copy number ratios close to normal, while all other tumor samples displayed significant copy number gain for this region (Fig. 4C). Two members of this gene cluster, *HIST2H4B* and *HIST2H2BE*, exhibited significant overexpression in osteosarcoma tumors (Fig. 4D) and also showed the smallest level of overexpression in T179. These results are indicative of the additive effects of genetic and epigenetic changes on gene expression at chromosome 1q.

In order to further validate our Me-DIP-Chip methylation array data, we performed quantitative mass spectrometry analysis on additional sets of differentially methylated regions (Supplementary Material, Table S3) including *HOM-TES-103* gene promoter (PGS detected as hypermethylated in T177, T178 relative to normal osteoblasts), *MAB21L2* gene promoter (PGS detected as hypermethylated in T179 and T180),

Downloaded from https://academic.oup.com/hmg/article/18/11/1962/2527323 by guest on 20 August 2022

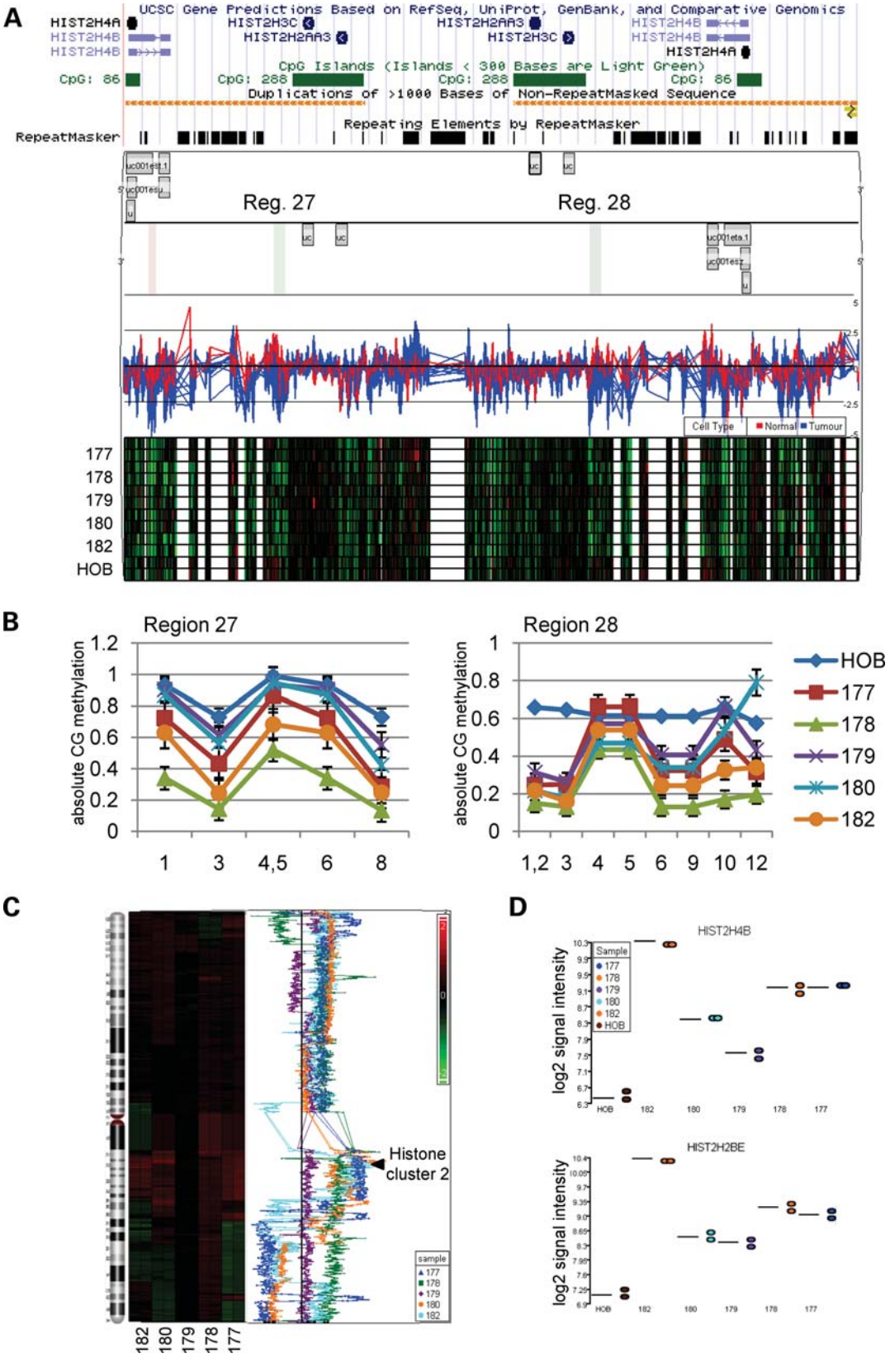

Downloaded from https://academic.oup.com/hmg/article/18/11/1962/2527323 by guest on 20 August 2022

STK32C and *LRRC27* gene promoter (PGS detected as hypomethylated), and negative control region at *STK17* gene promoter CpG island at transcriptional start site that showed no significant changes in PGS analysis (Supplementary Material, Fig. S3). Overall, these data show robust reproducibility of Me-DIP-Chip array data across 36 individual DNA sequences, and are representative of high-level heterogeneity in DNA methylation profiles of osteosarcoma tumors.

Fluorescence *in situ* hybridization validation of RUNX2 gain and DOCK5, TNFRSF10A and TNFRSF10D loss

Using integrative analysis we identified a strong correlation between tumor-specific copy number changes and gene expression (Figs 1B and 2B). Both integrative PGS microarray analysis and IPA gene network analysis point to *RUNX2* as the most significantly gained (6/10 tumors) and overexpressed (9-fold) gene locus at 6p12.3 (Supplementary Material, Table S5). *RUNX2* is also centrally involved in osteosarcoma oncogenesis transcriptional networks (Fig. 3B). Gene underexpression that was related to copy number loss was almost exclusively associated with chromosome 8p, where genes with the most significant loss included *DOCK5* (5/10 tumors), *TNFRSF10A* (4/10 tumors) and *TNFRSF10D* (4/10 tumors) and 6-, 3- and 3.5-fold underexpression, respectively (Supplementary Material, Table S5). Similar to *RUNX2*, both genes were strongly associated with transcriptional networks and functions implicated in osteosarcoma oncogenesis (Fig. 3A). We validated the results of our microarray analysis by performing a dual-color FISH of T180, which displayed a characteristically imbalanced copy number profile for all these loci. As a result, we show a high level copy number gain of the *RUNX2* gene locus (Fig. 5A and B), and a genomic loss (both hemi- and homozygous deletion) of *DOCK5* and *TNFRSF10A* and *TNFRSF10D* loci (Fig. 5C and D).

DISCUSSION

In this study, we provide one of the first fully integrated whole genome analyses of a human tumor at three levels (DNA copy number, transcriptome and promoter methylome) to delineate transcriptional networks leading to failure of osteoblast differentiation, onset of chromosomal instability and abrogation of apoptosis, while focusing on identification of genes involved in osteosarcoma-related gene networks. Our analysis shows high level of inter-tumor heterogeneity, in particular as it relates to the copy number and DNA methylation profiles as evident in the PCA profiles (Supplementary Material, Fig. S1). However, at the level of gene expression these tumors show striking similarity both globally (Supplementary Material, Fig. S1) as well as in relation to specific biological processes (Fig. 2C). Therefore, using a multilayered exclusion process, and by focusing on the identification of key genes belonging to the osteosarcoma-related gene expression networks we identified pathways that may be pivotal in the acquisition of the osteosarcoma tumor phenotype.

The power of integrating DNA copy number, methylome and transcriptome bioprofiles with gene network analysis provides a comprehensive screen for identification of pathways recurrently involved in osteosarcoma oncogenesis. Our overall analyses showed that DNA copy number is the best predictor of gene expression change. This strong effect of copy number change on expression is corroborated by evidence that genes with disruptions in all three profiles exhibited copy number gain, hypomethylation and gene overexpression in 49% of cases, while another 18% exhibited copy number gain, hypermethylation and gene overexpression (Fig. 1D). Group analyses of all three bioprofiles illustrated another general finding that DNA copy number gain correlated with promoter hypomethylation, and both were associated elevated expression. Cumulative analysis shows a correlation between copy number gain/loss and over/underexpression and hypomethylation and copy number gain (Fig. 2B). However, these molecular correlations are present in a relatively small proportion of the genes in any particular individual tumor sample (approximately 10–20% genes—compare Fig. 2B with Fig. 1B). This observation is expected because of a high level molecular heterogeneity that is observed in osteosarcoma, while identification of recurrent molecular aberrations, in particular ones that display concurrent deregulation of gene expression and are associated with osteosarcoma-related gene networks, may present the drivers of osteosarcoma tumorigenesis.

Molecular cytogenetic techniques together with the classical G-banded cytogenetic analysis of osteosarcoma tumors have described complex karyotypes with multiple numerical and structural chromosomal aberrations including high-level amplifications at 1q21, 6p21, 8q21-24, 12q13-q14 and 17p12-q11 (6–12). Our data are in keeping with these findings, in particular as it relates to the amplification of chromosome 1q21.1-q21.2, as well as the minimal region of gain at chromosome 6p12.3-p21.1. The identification of the copy number loss at chromosome 8p21.2-p21.3 is a novel finding that may be related to the superior sensitivity of the array-based assays used in this study, compared with the classical low resolution cytogenetic methods.

The most significant correlation between genomic gain and DNA hypomethylation was at chromosome 1q21 where seven genes were part of the histone cluster 2 gene family at 1q21.1-q21.2; *HIST2H2BE* and *HIST2H4B* were significantly

Figure 4. Correlation of DNA hypomethylation of histone cluster 2 at 1q21 with copy number gain and gene overexpression. (**A**) PGS-detection of extensive hypomethylation at 1q21 histone cluster 2. From top to bottom, UCSC Genome Browser gene, CpG island and genomic repeat tracks are shown overlayed with the PGS visualization of gene tracks, regions detected as significantly hypomethylated in PGS, PGS profile of normal versus tumor DNA methylation signal, and PGS heat-maps of duplicate array signals for DNA methylation enrichment in a green (depletion relative to input) to red (enrichment relative to input) gradient in tumor samples and normal osteoblasts. (**B**) Validation of DNA hypomethylation at 1q21 histone cluster 2. Graphs show quantitative EpiTYPER analysis of DNA methylation at individual CpG dinucleotides at PGS-detected regions of significant hypomethylation 27 and 28 (Fig. 5A; Supplementary Material, Table S3). (**C**) Copy number gain of 1q21. PGS visualization of copy number gain region 1q21 (Supplementary Material, Table S2) showing a heat map (replicate arrays), and profile visualizations in tumor samples. (**D**) Overexpression of histone cluster 2 genes. PGS dot plot visualization of significantly overexpressed histone gene variants (Supplementary Material, Table S1) from histone cluster 2 at 1q21. Average signal across gene-specific probe set for *HIST2H4B* and *HIST2H2BE* variants for each replicate and bar denoting the mean are shown for each tumor and normal sample. *Y*-axis represents the raw log2 signal intensity for each probe set.

Downloaded from https://academic.oup.com/hmg/article/18/11/1962/2527323 by guest on 20 August 2022

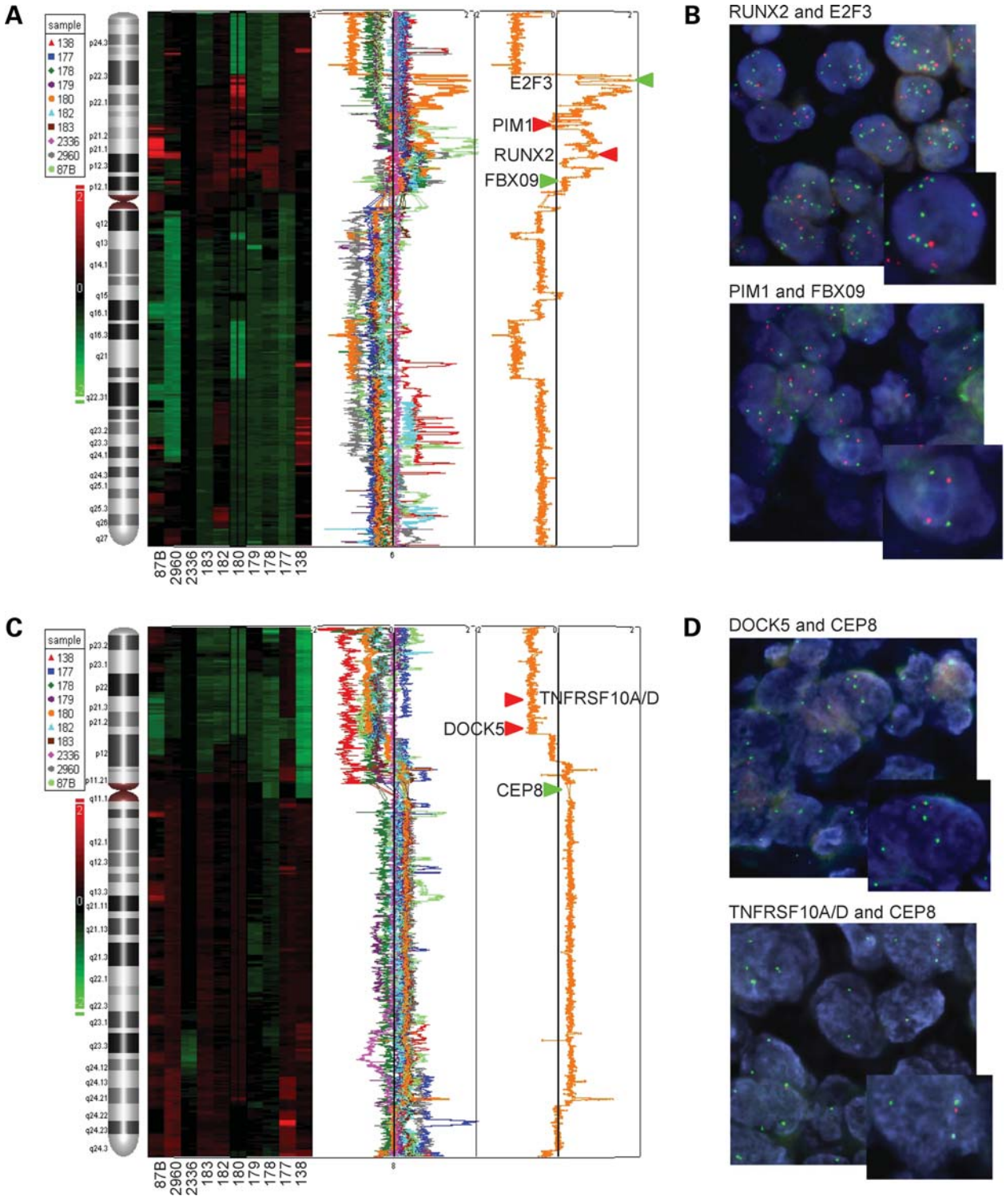

Figure 5. Amplification of *RUNX2*, and loss of *DOCK5*, *TNFRSF10A* and *TNFRSF10D* loci. (**A**) PGS visualization of the heat map (replicate arrays) and profile view of the 10 tumor samples, and profile view of T180, including the most significantly gained and overexpressed (Supplementary Material, Tables S1, S2 and S4) putative oncogene *RUNX2* locus, and *E2F3*, *PIM1* and *FBX09* control fluorescence *in situ* hybridization (FISH) loci. Green and red arrows denote exact chromosomal loci and FISH color. (**B**) Validation of *RUNX2* locus amplification. Representative images of FISH analysis of *RUNX2* and *E2F3* loci (top panel), and *PIM1* and *FBX09* loci (bottom panel) in osteosarcoma sample T180. (**C**) PGS visualization of the heat map (replicate arrays) and profile view of the 10 tumor samples, and profile view of T180, including the most significantly lost and underexpressed (Supplementary Material, Tables S1, S2 and S4) putative tumor suppressor *DOCK5* and *TNFRSF10A/D* loci and control CEP8 locus. Green and red arrows denote exact chromosomal loci and FISH color. (**D**) Validation of *DOCK5* and *TNFRSF10A/D* loss of heterozygosity. Representative images of FISH analysis of *DOCK5* and CEP8 loci (top panel), and *TNFRSF10A/D* and CEP8 loci (bottom panel) in osteosarcoma sample T180.

Downloaded from https://academic.oup.com/hmg/article/18/11/1962/2527323 by guest on 20 August 2022

overexpressed, and *HIST2H2BE* has a central role in the most significant gene network involved in organ and cell development. Quantitative analysis of promoter methylation in this region confirmed these findings while providing additional evidence of correlation and cumulative effects of hypomethylation and genomic gain together with concordant elevated gene expression (Fig. 4).

Chromosome 1q gain is a frequent event in many malignancies, but it is not clear what the candidate genes in this region may be. Integrative bioprofiling and gene network analyses suggest that gain of Histone cluster 2 gene family may confer a beneficial selective advantage during tumorigenesis. In addition to the structural role related to chromatin assembly, there is a growing appreciation of the role of histones in chromatin-based processes and epigenetic regulation, including the deposition of histone variants and nucleosome remodeling (23).

The region with the most significant copy number loss was chromosome 8p21.2-p21.3. Integrative bioprofile analysis and identification of interactive networks showed that dedicator of cytokinesis 5 (*DOCK5*) and tumor necrosis factor receptor superfamily members 10A and 10D (*TNFRSF10A* and *TNFRSF10D*) had the most significant loss and associated underexpression in our tumor cohort (Supplementary Material, Fig. S4; Table 1). In a recent study, Brazier and coworkers (24) provided evidence that *DOCK5* expression is essential for bone differentiation, from precursor osteoclasts. The loss of the apoptosis regulator p53 is very common in osteosarcoma (25–27), and loss of expression of *TP53* is evident as the central feature of the cancer and cell death-related expression network in our study (Fig. 3A), suggesting that deregulation of this pathway is essential in osteosarcoma. Further support for this hypothesis involves *TNFRSF10A* and *TNFRSF10D* genes, which together with *DOCK5* are significantly lost and underexpressed in our tumor cohort (Supplementary Material, Fig. S4; Table 1). *TNFRSF10A* is a receptor activated by tumor necrosis factor-related apoptosis inducing ligand *TNFSF10* (also known as TRAIL), which transduces cell death signal, induces cell apoptosis and is a potential target for development of agonistic TRAIL-like chemotherapeutics (28). Interestingly, this pathway is mostly p53-independent, but there is some evidence of p53-dependent activation of *TNFRSF10A* (21). Collectively, these data show that the most significant region of copy number loss and gene underexpression of chromosome 8p21.2-p21.3 may play a dual role in acquisition of the osteosarcoma phenotype, by disrupting bone differentiation through *DOCK5* and disruption of p53-altenate cell death pathways through *TNFRSF10A*.

Amplification-related overexpression of *RUNX2* at chromosome 6p12.3-p21.1 leads to constitutive promotion of *RUNX2* gene expression. This gene is also essential for bone differentiation, and is located centrally within the most significant region of amplification chromosome 6p (Fig. 3B; Table 1). These two cytobands have been previously identified as common regions of gain in osteosarcoma using classical cytogenetic and low resolution microarray approaches (6–8,10,22,29). In a recent study that utilized bacterial artificial chromosomes (BAC) arrays, the consensus part of the region of amplification was found to be approximately 7.9 Mb, and it included *RUNX2* among 11 other candidate genes that may be involved in osteosarcoma (30). In this study we find that the smallest region of amplification is approximately 1 Mb (Fig. 5A; Supplementary Material, Table S4), and in combination with integrative expression profiling and network analysis, we identify *RUNX2* as the strongest candidate gene having a direct role in osteosarcoma oncogenesis. The family of *Runx* genes (includes *RUNX1* and *RUNX3*) are differentiation mediators that are expressed at different stages of osteoblast development. Their function in cell cycle checkpoints and cell division control is crucial because loss of function can lead to acquisition of polyploidization (one of the characteristic features of osteosarcoma). *RUNX2* expression is essential for mesenchymal stem cell differentiation along the osteoblast lineage and bone development (31), but overexpression of *RUNX2* in lineage-restricted osteoblasts blocks terminal differentiation to osteocytes and increases bone resorption (32,33). This indicates that *RUNX2* is necessary for osteoblast lineage specification from mesenchymal precursors, but its levels must be tightly regulated in determined osteocytic cells (34). This dual role of *RUNX2* is exemplified by the finding that *RUNX2*, in combination with *HDAC6*, represses the cell cycle checkpoint-related p21 (35) while another group provided evidence suggesting that *RUNX2* is involved in the establishment of terminal differentiation in osteoblasts by inducing Rb- and p27-dependent growth arrest (36). Therefore, *RUNX2* is required for the initiation of transition of mesenchymal stem cells to the osteoblast lineage as well as termination of osteoblast lineage expansion and terminal differentiation. Recent reviews describe oncogenic properties of *RUNX2* that include induction of lymphomas in mice, transformation of p53-null fibroblasts, induction of T-cell lymphoma and a regulatory role in breast and prostate cancer metastasis to bone (34,37). Although RUNX2 is involved in a number of signaling pathways, including Wnt signaling, FGF signaling and extracellular matrix signaling, it plays a particularly important role in the mediation of BMP/TGF-beta growth and differentiation signaling pathway that is hyperactive in the majority of tumors (37). Together, these studies corroborate the evidence of the role of RUNX2 in pro-growth pathways and disruption of terminal differentiation and cell cycle regulatory factors involved in bone morphogenesis and acquisition of aneuploidy. Our data are consistent with this, which is clearly evident in the IPA Gene Neighborhood Analysis of *RUNX2* in the expression data set (Fig. 6A). This analysis shows the *RUNX2* interactome map of all genes detected as differentially expressed in our tumor samples, known to biologically interact with *RUNX2* and are involved in *RUNX2* signaling. It shows evidence of strong activation of both BMP and TGF-beta pathways, as well as the concurrent inactivation of the cell cycle checkpoint and DNA damage pathway that includes p53, p21 (CDKN1) and CCNB1.

Collectively, these reports and the data presented in this study provide compelling reasons to consider constitutive activation of *RUNX2* to be of high relevance in osteosarcoma oncogenesis (Fig. 6B). The constitutive promotion of *RUNX2* gene expression could disrupt G2/M cell cycle checkpoints, and downstream osteosarcoma-specific changes such as failure of bone differentiation and genomic polyploidization. Similarly, failure of *DOCK5*-signaling, together with

Downloaded from https://academic.oup.com/hmg/article/18/11/1962/2527323 by guest on 20 August 2022

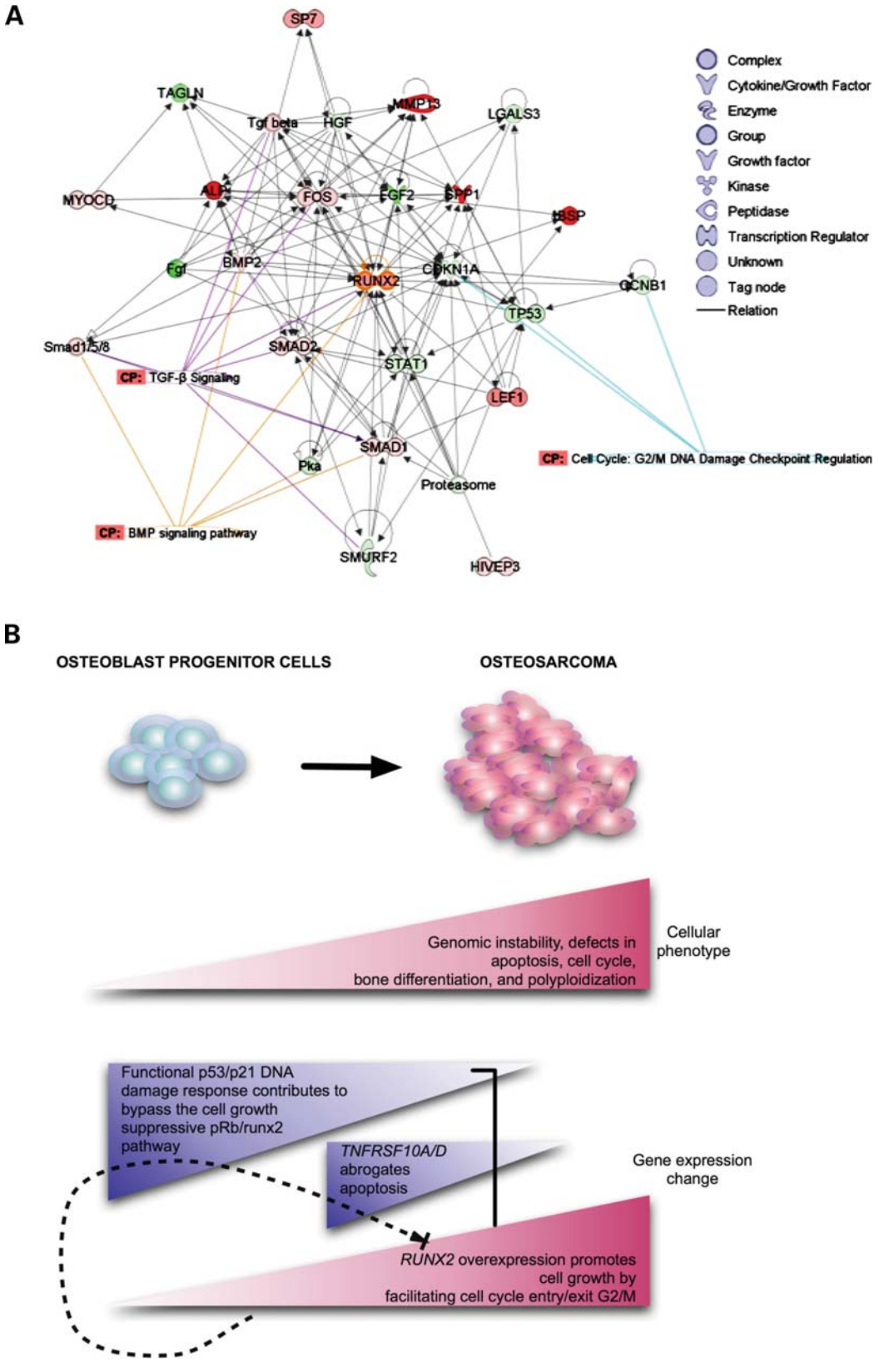

Figure 6. Involvement of *RUNX2* in pro-growth pathways and disruption of cell cycle checkpoints. (**A**) Gene network view of the *RUNX2* neighborhood analysis using Ingenuity Pathway Analysis (IPA) from the OS-specific gene expression profiling (cumulative analysis). Red and green signify gain or loss of gene expression, and arrows denote gene-specific relationships according to IPA knowledge database of genes that interact with *RUNX2*. The colored lines connect members of the specific canonical pathways, including TGF-β signaling, BMP signaling and G2/M DNA damage checkpoint regulation. (**B**) Model of *RUNX2*-related oncogenesis in osteosarcoma.

Downloaded from https://academic.oup.com/hmg/article/18/11/1962/2527323 by guest on 20 August 2022

p53- and *TNFRSF10A/D*-related cell cycle and death pathways, may play a critical role in abrogating apoptosis in this tumor.

MATERIALS AND METHODS

Tumor tissue samples and osteoblast DNA and RNA extraction

The 10 pediatric osteosarcoma samples were obtained from treatment of naïve tumor biopsies, and had institutional review board approval. Normal human osteoblasts were purchased from PromoCell (Heidelberg, Germany, Catalogue no. C-12760). Genomic DNA was extracted from tissue digested in a proteinase K buffer and purified by standard phenol/chloroform methods. Total RNA was extracted using the TRIzol Reagent method according to the manufacturer's protocol (Invitrogen, Carlsbad, CA, USA), and quantitated using bio-analyzer (Agilent Technologies Inc., Palo Alto, CA, USA).

Me-DIP-chip

Analysis of genomic methylation was performed by methylated DNA immunoprecipitation followed by the microarray hybridization (Me-DIP-chip) using the Affymetrix Human Promoter 1.0R Tilling Arrays using a modification of the Affymetrix chromatin immunoprecipitation assay as previously described (20). Random priming reactions of totally 50 ng of IP and IN DNA, followed by the genomic polymerase chain reaction, were performed using a modification of the Affymetrix chromatin immunoprecipitation assay protocol as previously described (38). Array hybridization and scanning were performed at the Centre for Applied Genomics (The Hospital for Sick Children, Toronto, ON, Canada). All microarray experiments were performed in duplicates for both IP and IN fractions of each DNA sample starting with initial sonication step.

Array-CGH

The Agilent Human Genome 244K CGH microarray (Agilent Technologies) were used for copy number analysis as previously described (12). Dye-swapped duplicate experiments were carried out for all samples.

Expression arrays

Genomic RNA expression analysis was performed using the Affymetrix Gene 1.0 ST arrays. RNA (200 ng) from normal human osteoblasts and tumor samples was analyzed as per manufacturer's instructions at the Centre for Applied Genomics (The Hospital for Sick Children). Each experiment was performed in duplicates.

Data analysis and integration

Data from Me-DIP-chip and RNA expression array experiments in the form of .cel files (GCOS 1.3 software), and a-CGH.txt files (Agilent Feature Extraction software) were imported into, analyzed and integrated using the PGS Software according to the previously described protocol (20) with following modifications and parameters:

The analysis of Me-DIP-Chip data included following Hidden Markov Model (HMM) parameters: s-HMM (min. probes: 10, detection states: $-5,5$, ignore state: 0, max. probability: 0.99, genomic decay: 10 000, sigma: 2); m-HMM (min. probes: 15, detection states: $-3,3$, ignore state: 0, max. probability: 0.99, genomic decay: 10 000, sigma: 1); l-HMM (min. probes: 40, detection states: $-1.5,1.5$, ignore state: 0, max. probability: 0.99, genomic decay: 10 000, sigma: 1). Significantly enriched/hypermethylated and depleted/hypomethylated HMM regions were annotated to the corresponding genes present on the Affymetrix Gene 1.0 Array using the HuGene-1_0-st-v1.na24.hg18.transcriptmod.csv file, which was annotated to detect regions associated with specific genes 10 kb 5′ and 3 kb 3′ from transcriptional start sites to correspond to the coverage on the Affy Promoter 1.0R Array.

The analysis of expression data utilized one-way analysis of variance (ANOVA) tool at $P < 0.01$ and ± 2-fold enrichment, either specifically for each tumor sample or cumulatively (i.e. mean signal of all tumors versus osteoblasts). Significantly over- and underexpressed genes were annotated using Affymetrix Gene 1.0 Array using the HuGene-1_0-st-v1.na24.hg18.transcript.csv file.

The analysis of copy number utilized Genomic Segmentation tool with parameters set at: min. probes: 10, *P*-value threshold: 0.01 and signal to noise: 0.1. Region report was set at values below $-0.5/+0.5$ ($\log_2$) and *P*-value threshold of 0.05 for 2/2 (replicate) arrays in individual analysis or at 40% cut-off in cumulative analysis (i.e. 4/10 tumor samples). Regions of significant gain or loss were annotated to the corresponding genes present on the Affymetrix Gene 1.0 Array using the HuGene-1_0-st-v1.na24.hg18.transcript.csv file.

In order to determine the relative enrichment, we used the PGS one-way ANOVA tool and calculate the fold change using the geometric mean (for log-transformed data) for individual tumors, or alternatively for all tumors versus osteoblasts (cumulative analysis) for gene expression and methylation, and using Genomic Segmentation algorithm for copy number analysis. The integration of significantly hypo- and hypermethylated, over- and underexpressed, and gained and lost gene lists was performed using the VENN tool in PGS, and visualization to the resulting tracks was performed as previously described (38). Copy number and DNA methylation analysis excluded sex chromosomes to avoid bias in the identification of significant genes/regions owing to sex differences between some tumor samples and male human osteoblast controls.

Network identification and canonical pathway analysis

Functional identification of gene networks was performed using IPA program as previously described (38). The .xls tables representing the differentially expressed, methylated and genomically imbalanced genes from tumor samples as well as the corresponding expression (relative to osteoblasts), methylation enrichment (mean of regions associated with individual gene, relative to osteoblasts), and gain ($+1$) and loss (-1) for tumor-specific, or ($\pm$no. of arrays) for cumulative analyses copy number values were imported as individual

Downloaded from https://academic.oup.com/hmg/article/18/11/1962/2527323 by guest on 20 August 2022

experiments using the Core Analysis tool. The analysis was performed using Ingenuity Knowledge Database and was limited to direct interactions only.

Quantitative mass-spectrometric CPG methylation analysis

We used EpiTYPER MassARRAY System (Sequenom, USA) for quantitative DNA methylation analysis at the Analytical Genetics Technology Centre (Princess Margaret Hospital, Toronto, ON, Canada), as per manufacturer's instructions (http://www.analyticalgenetics.ca/Function/Business/Service/Methylation.aspx), using the original DNA samples from the Me-DIP-chip experiment. The bisulfite primers (Supplementary Material, Table S9) were designed to overlap HMM-detected regions of differential enrichment, or regions of no significant changes as controls, using the MethPrimer Software (http://www.urogene.org/methprimer/index1.html). Analyses were performed in triplicate and all resolvable CpG signals were mapped and standard error bars are displayed.

Fluorescence *in situ* hybridization

BAC clones were selected for locus-specific regions (Supplementary Material, Table S10), whereas commercially available DNA probe for the centromeric region 8p11.1-q11.1 (SpectrumGreen labeled CEP 8—Vysis Inc., Downers Grove, IL, USA) was used as control for the locus-specific and ploidy analyses. The presence of the target locus-specific sequences and correct chromosome location of the BAC clones were verified by PCR and by hybridization to metaphase spreads from normal peripheral lymphocytes, respectively. BAC DNA was extracted and labeled with either Spectrum Green–dUTP or SpectrumOrange–dUTP, using the nick-translation kit (Vysis Inc.). Five micrometer histological formalin-fixed and paraffin-embedded tissue sections were deparaffinized with a series of xylene prior to immersion in 100% ethanol. FISH was carried out as described (39). Copy number change was evaluated for each probe by counting spots in 200 non-overlapped, intact interphase nuclei per tumor tissue section using a Zeiss Imager.Z1 microscope. The establishment of genomic gain and amplification for *RUNX2* were defined considering the adjacent probes (*E2F3*, *PIM1* and *FBXO9* loci) used for the truncation artifacts, aneusomy, nuclear size and chromatin condensation (40). Similarly, the establishment of *DOCK5*, *TNFRSF10D* and *TNFRSF10A* gene copy number status was defined by considering the CEP 8 DNA probe (Vysis, Inc.) (40).

Accession numbers

The Gene Expression Omnibus (GEO) (http://www.ncbi.nlm.nih.gov/geo) series accession number discussed in this paper is GSE12830.

SUPPLEMENTARY MATERIAL

Supplementary Material is available at *HMG* online.

ACKNOWLEDGEMENTS

B.S. is a Fellow of the National Cancer Institute of Canada (Terry Fox Foundation) and Restracomp Fellow at the Hospital for Sick Children, Toronto, Canada.

Conflict of Interest statement. None declared.

FUNDING

This research is funded by the Canadian Cancer Society (grant no. 016215).

REFERENCES

1. Hanahan, D. and Weinberg, R.A. (2000) The hallmarks of cancer. *Cell*, **100**, 57–70.
2. Sadikovic, B., Al-Romaih, K., Squire, J. and Zielenska, M. (2008) Cause and consequences of genetic and epigenetic alterations in human cancer. *Curr. Genomics*, **9**, 394–408.
3. Kondo, Y., Shen, L., Cheng, A.S., Ahmed, S., Boumber, Y., Charo, C., Yamochi, T., Urano, T., Furukawa, K., Kwabi-Addo, B. *et al.* (2008) Gene silencing in cancer by histone H3 lysine 27 trimethylation independent of promoter DNA methylation. *Nat. Genet.*, **40**, 741–750.
4. McLendon, R., Friedman, A., Bigner, D., Van Meir, E.G., Brat, D.J., Mastrogianakis, M., Olson, J.J., Mikkelsen, T., Lehman, N., Aldape, K. *et al.* (2008) Comprehensive genomic characterization defines human glioblastoma genes and core pathways. *Nature*.
5. Parsons, D.W., Jones, S., Zhang, X., Lin, J.C., Leary, R.J., Angenendt, P., Mankoo, P., Carter, H., Siu, I.M., Gallia, G.L. *et al.* (2008) An integrated genomic analysis of human glioblastoma multiforme. *Science*, **321**, 1807–1812.
6. Batanian, J.R., Cavalli, L.R., Aldosari, N.M., Ma, E., Sotelo-Avila, C., Ramos, M.B., Rone, J.D., Thorpe, C.M. and Haddad, B.R. (2002) Evaluation of paediatric osteosarcomas by classic cytogenetic and CGH analyses. *Mol. Pathol.*, **55**, 389–393.
7. Lim, G., Karaskova, J., Beheshti, B., Vukovic, B., Bayani, J., Selvarajah, S., Watson, S.K., Lam, W.L., Zielenska, M. and Squire, J.A. (2005) An integrated mBAND and submegabase resolution tiling set (SMRT) CGH array analysis of focal amplification, microdeletions, and ladder structures consistent with breakage-fusion-bridge cycle events in osteosarcoma. *Genes Chromosomes Cancer*, **42**, 392–403.
8. Lim, G., Karaskova, J., Vukovic, B., Bayani, J., Beheshti, B., Bernardini, M., Squire, J.A. and Zielenska, M. (2004) Combined spectral karyotyping, multicolor banding, and microarray comparative genomic hybridization analysis provides a detailed characterization of complex structural chromosomal rearrangements associated with gene amplification in the osteosarcoma cell line MG-63. *Cancer Genet. Cytogenet.*, **153**, 158–164.
9. Sandberg, A.A. and Bridge, J.A. (2003) Updates on the cytogenetics and molecular genetics of bone and soft tissue tumors: osteosarcoma and related tumors. *Cancer Genet. Cytogenet.*, **145**, 1–30.
10. Squire, J.A., Pei, J., Marrano, P., Beheshti, B., Bayani, J., Lim, G., Moldovan, L. and Zielenska, M. (2003) High-resolution mapping of amplifications and deletions in pediatric osteosarcoma by use of CGH analysis of cDNA microarrays. *Genes Chromosomes Cancer*, **38**, 215–225.
11. Zielenska, M., Marrano, P., Thorner, P., Pei, J., Beheshti, B., Ho, M., Bayani, J., Liu, Y., Sun, B.C., Squire, J.A. *et al.* (2004) High-resolution cDNA microarray CGH mapping of genomic imbalances in osteosarcoma using formalin-fixed paraffin-embedded tissue. *Cytogenet. Genome Res.*, **107**, 77–82.
12. Selvarajah, S., Yoshimoto, M., Maire, G., Paderova, J., Bayani, J., Squire, J.A. and Zielenska, M. (2007) Identification of cryptic microaberrations in osteosarcoma by high-definition oligonucleotide array comparative genomic hybridization. *Cancer Genet. Cytogenet.*, **179**, 52–61.
13. Locklin, R.M., Oreffo, R.O. and Triffitt, J.T. (1998) Modulation of osteogenic differentiation in human skeletal cells *in vitro* by 5-azacytidine. *Cell Biol. Int.*, **22**, 207–215.

Downloaded from https://academic.oup.com/hmg/article/18/11/1962/2527323 by guest on 20 August 2022

14. Ryhanen, S., Pirskanen, A., Jaaskelainen, T. and Maenpaa, P.H. (1997) State of methylation of the human osteocalcin gene in bone-derived and other types of cells. *J. Cell. Biochem.*, **66**, 404–412.
15. Villagra, A., Gutierrez, J., Paredes, R., Sierra, J., Puchi, M., Imschenetzky, M., Wijnen, Av.A., Lian, J., Stein, G., Stein, J. *et al.* (2002) Reduced CpG methylation is associated with transcriptional activation of the bone-specific rat osteocalcin gene in osteoblasts. *J. Cell. Biochem.*, **85**, 112–122.
16. Harada, K., Toyooka, S., Maitra, A., Maruyama, R., Toyooka, K.O., Timmons, C.F., Tomlinson, G.E., Mastrangelo, D., Hay, R.J., Minna, J.D. *et al.* (2002) Aberrant promoter methylation and silencing of the *RASSF1A* gene in pediatric tumors and cell lines. *Oncogene*, **21**, 4345–4349.
17. Ulaner, G.A., Vu, T.H., Li, T., Hu, J.F., Yao, X.M., Yang, Y., Gorlick, R., Meyers, P., Healey, J., Ladanyi, M. *et al.* (2003) Loss of imprinting of IGF2 and H19 in osteosarcoma is accompanied by reciprocal methylation changes of a CTCF-binding site. *Hum. Mol. Genet.*, **12**, 535–549.
18. Al-Romaih, K., Sadikovic, B., Yoshimoto, M., Wang, Y., Zielenska, M. and Squire, J.A. (2008) Decitabine-induced demethylation of 5′ CpG island in GADD45A leads to apoptosis in osteosarcoma cells. *Neoplasia*, **10**, 471–480.
19. Al-Romaih, K., Somers, G.R., Bayani, J., Hughes, S., Prasad, M., Cutz, J.C., Xue, H., Zielenska, M., Wang, Y. and Squire, J.A. (2007) Modulation by decitabine of gene expression and growth of osteosarcoma U2OS cells *in vitro* and in xenografts: identification of apoptotic genes as targets for demethylation. *Cancer Cell Int.*, **7**, 14.
20. Sadikovic, B., Yoshimoto, M., Al-Romaih, K., Maire, G., Zielenska, M. and Squire, J.A. (2008) *In vitro* analysis of integrated global high-resolution DNA methylation profiling with genomic imbalance and gene expression in osteosarcoma. *PLoS ONE*, **3**, e2834.
21. Bartke, T., Siegmund, D., Peters, N., Reichwein, M., Henkler, F., Scheurich, P. and Wajant, H. (2001) p53 upregulates cFLIP, inhibits transcription of NF-kappaB-regulated genes and induces caspase-8-independent cell death in DLD-1 cells. *Oncogene*, **20**, 571–580.
22. Forus, A., Weghuis, D.O., Smeets, D., Fodstad, O., Myklebost, O. and Geurts van Kessel, A. (1995) Comparative genomic hybridization analysis of human sarcomas: II. Identification of novel amplicons at 6p and 17p in osteosarcomas. *Genes Chromosomes Cancer*, **14**, 15–21.
23. Henikoff, S. (2008) Nucleosome destabilization in the epigenetic regulation of gene expression. *Nat. Rev. Genet.*, **9**, 15–26.
24. Brazier, H., Stephens, S., Ory, S., Fort, P., Morrison, N. and Blangy, A. (2006) Expression profile of RhoGTPases and RhoGEFs during RANKL-stimulated osteoclastogenesis: identification of essential genes in osteoclasts. *J. Bone Miner. Res.*, **21**, 1387–1398.
25. Gokgoz, N., Wunder, J.S., Mousses, S., Eskandarian, S., Bell, R.S. and Andrulis, I.L. (2001) Comparison of p53 mutations in patients with localized osteosarcoma and metastatic osteosarcoma. *Cancer*, **92**, 2181–2189.
26. Miller, C.W., Aslo, A., Tsay, C., Slamon, D., Ishizaki, K., Toguchida, J., Yamamuro, T., Lampkin, B. and Koeffler, H.P. (1990) Frequency and structure of p53 rearrangements in human osteosarcoma. *Cancer Res.*, **50**, 7950–7954.
27. Radig, K., Schneider-Stock, R., Oda, Y., Neumann, W., Mittler, U. and Roessner, A. (1996) Mutation spectrum of *p53* gene in highly malignant human osteosarcomas. *Gen. Diagn. Pathol.*, **142**, 25–32.
28. Carlo-Stella, C., Lavazza, C., Locatelli, A., Vigano, L., Gianni, A.M. and Gianni, L. (2007) Targeting TRAIL agonistic receptors for cancer therapy. *Clin. Cancer Res.*, **13**, 2313–2317.
29. Zielenska, M., Bayani, J., Pandita, A., Toledo, S., Marrano, P., Andrade, J., Petrilli, A., Thorner, P., Sorensen, P. and Squire, J.A. (2001) Comparative genomic hybridization analysis identifies gains of 1p35 approximately p36 and chromosome 19 in osteosarcoma. *Cancer Genet. Cytogenet.*, **130**, 14–21.
30. Lu, X.Y., Lu, Y., Zhao, Y.J., Jaeweon, K., Kang, J., Xiao-Nan, L., Ge, G., Meyer, R., Perlaky, L., Hicks, J. *et al.* (2008) Cell cycle regulator gene CDC5L, a potential target for 6p12-p21 amplicon in osteosarcoma. *Mol. Cancer Res.*, **6**, 937–946.
31. Byers, B.A. and Garcia, A.J. (2004) Exogenous Runx2 expression enhances *in vitro* osteoblastic differentiation and mineralization in primary bone marrow stromal cells. *Tissue Eng.*, **10**, 1623–1632.
32. Geoffroy, V., Kneissel, M., Fournier, B., Boyde, A. and Matthias, P. (2002) High bone resorption in adult aging transgenic mice overexpressing cbfa1/runx2 in cells of the osteoblastic lineage. *Mol. Cell. Biol.*, **22**, 6222–6233.
33. Liu, W., Toyosawa, S., Furuichi, T., Kanatani, N., Yoshida, C., Liu, Y., Himeno, M., Narai, S., Yamaguchi, A. and Komori, T. (2001) Overexpression of Cbfa1 in osteoblasts inhibits osteoblast maturation and causes osteopenia with multiple fractures. *J. Cell Biol.*, **155**, 157–166.
34. Schroeder, T.M., Jensen, E.D. and Westendorf, J.J. (2005) Runx2: a master organizer of gene transcription in developing and maturing osteoblasts. *Birth Defects Res. C. Embryo Today*, **75**, 213–225.
35. Westendorf, J.J., Zaidi, S.K., Cascino, J.E., Kahler, R., van Wijnen, A.J., Lian, J.B., Yoshida, M., Stein, G.S. and Li, X. (2002) Runx2 (Cbfa1, AML-3) interacts with histone deacetylase 6 and represses the p21(CIP1/WAF1) promoter. *Mol. Cell. Biol.*, **22**, 7982–7992.
36. Thomas, D.M., Johnson, S.A., Sims, N.A., Trivett, M.K., Slavin, J.L., Rubin, B.P., Waring, P., McArthur, G.A., Walkley, C.R., Holloway, A.J. *et al.* (2004) Terminal osteoblast differentiation, mediated by runx2 and p27KIP1, is disrupted in osteosarcoma. *J. Cell Biol.*, **167**, 925–934.
37. Pratap, J., Lian, J.B., Javed, A., Barnes, G.L., van Wijnen, A.J., Stein, J.L. and Stein, G.S. (2006) Regulatory roles of Runx2 in metastatic tumor and cancer cell interactions with bone. *Cancer Metastasis Rev.*, **25**, 589–600.
38. Sadikovic, B., Andrews, J., Carter, D., Robinson, J. and Rodenhiser, D.I. (2008) Genome-wide H3K9 histone acetylation profiles are altered in benzopyrene-treated MCF7 breast cancer cells. *J. Biol. Chem.*, **283**, 4051–4060.
39. Yoshimoto, M., Cunha, I.W., Coudry, R.A., Fonseca, F.P., Torres, C.H., Soares, F.A. and Squire, J.A. (2007) FISH analysis of 107 prostate cancers shows that PTEN genomic deletion is associated with poor clinical outcome. *Br. J. Cancer*, **97**, 678–685.
40. Ventura, R.A., Martin-Subero, J.I., Jones, M., McParland, J., Gesk, S., Mason, D.Y. and Siebert, R. (2006) FISH analysis for the detection of lymphoma-associated chromosomal abnormalities in routine paraffin-embedded tissue. *J. Mol. Diagn.*, **8**, 141–151.

Downloaded from https://academic.oup.com/hmg/article/18/11/1962/2527323 by guest on 20 August 2022